Jean Hamilton, Matthew A. Nunes, Marina I. Knight, and Piotr Fryzlewicz

Complex-valued wavelet lifting and applications

Article (Accepted version)
(Refereed)

Complex-valued wavelet lifting and applications

Jean Hamilton
HEDS, ScHARR, University of Sheffield
Matthew A. Nunes*
Department of Mathematics and Statistics, Lancaster University
Marina I. Knight
Department of Mathematics, University of York
and
Piotr Fryzlewicz
Department of Statistics, London School of Economics

January 10, 2017

Abstract

Signals with irregular sampling structures arise naturally in many fields. In applications such as spectral decomposition and nonparametric regression, classical methods often assume a regular sampling pattern, thus cannot be applied without prior data processing. This work proposes new complex-valued analysis techniques based on the wavelet lifting scheme that removes 'one coefficient at a time'. Our proposed lifting transform can be applied directly to irregularly sampled data and is able to adapt to the signal(s)' characteristics. As our new lifting scheme produces complex-valued wavelet coefficients, it provides an alternative to the Fourier transform for irregular designs, allowing phase or directional information to be represented. We discuss applications in bivariate time series analysis, where the complex-valued lifting construction allows for coherence and phase quantification. We also demonstrate the potential of this flexible methodology over real-valued analysis in the nonparametric regression context.

Keywords: lifting scheme; wavelets; nondecimated transform; (bivariate) time series; coherence and phase; nonparametric regression.

---

*Corresponding author: `m.nunes@lancaster.ac.uk`

1   Introduction

Since the early nineties, wavelets have become a popular tool for nonparametric regression, statistical image processing and time series analysis. In particular, due to their natural localisation, wavelets can provide sparse representations for certain functions that cannot be represented efficiently using Fourier sinusoids. Reviews of the use of wavelets in statistics include Nason (2008) and Abramovich et al. (2000).

Until recently, the majority of work in the statistical literature has been based on the discrete wavelet transform (DWT). However, classical wavelet methods suffer from some limitations; in particular, usage is restricted to data sampled at regular time or spatial locations, and a dyadic data dimension is often imposed. Wavelet lifting (Sweldens, 1996) can be used to overcome many of the shortcomings of the standard DWT. Specifically, wavelet functions obtained through the wavelet lifting scheme provide an extension of classical wavelet methods to more general settings, such as irregularly sampled data.

On the other hand, it is now well-established that *complex-valued* data analysis tools can extract useful information that is potentially missed when using traditional real-valued wavelet techniques, even for real-valued data, see for example Lina and Mayrand (1995); Fernandes et al. (2003); Selesnick et al. (2005). In particular, using complex-valued multiscale methods has been advantageous in a range of statistical applications such as nonparametric regression (Barber and Nason, 2004), image processing (Kingsbury, 1999; Portilla and Simoncelli, 2000) and time series analysis (Magarey and Kingsbury, 1998; Kingsbury, 2001).

Complex-valued multiscale techniques building upon the lifting scheme as introduced by Sweldens (1996) have been introduced in the literature by Abbas and Tran (2006), who briefly investigated their proposed technique in the image denoising context, and by Shui et al. (2003), who focused on the design of complex filters with desired band-pass properties.

This article introduces a new *adaptive complex-valued wavelet lifting scheme* built upon the lifting 'one coefficient at a time' (LOCAAT) framework of Jansen et al. (2001, 2009). A *nondecimated* variant of the proposed transform, which allows for an overcomplete representation of such data is also introduced. The added benefits of our methodology are: (i) flexibility – it can be applied to irregularly sampled grids of (possibly) non-dyadic length; (ii) information augmentation – through the *complex-valued* wavelet coefficients, the scheme

2

exploits additional signal information not used by real-valued transforms; and (iii) applicability – it allows for the analysis of bivariate nonstationary signals with possibly different (irregular) sampling structures, previously not directly possible using methods currently in the literature.

We demonstrate the benefits of our new technique for spectral estimation of irregularly sampled time series, with a particular focus on coherence and phase quantification for irregularly sampled bivariate time series. In this context, the methodology can be viewed as a wavelet lifting analogue to the Fourier transform and can be used for the same purposes. The good performance of our method is also displayed in the nonparametric regression setting.

The paper is organised as follows. Section 2 introduces the new complex-valued lifting algorithm, including its overcomplete variant. Section 3 details the application of the complex-valued lifting algorithm to discover local frequency content of irregularly sampled uni- and bivariate time series. Section 4 tackles nonparametric regression for (real-valued) signals.

2 The complex-valued lifting scheme

The lifting scheme (Sweldens, 1996) was introduced as a flexible way of providing wavelet-like transforms for *irregular* data. Lifting bases are naturally compactly supported, and via the recursive nature of the transform, one can build wavelets with desired properties, such as vanishing moments. In addition, lifting algorithms are known to be computationally faster than traditional wavelet transforms since they require fewer computations compared with classical transforms. For an overview of the lifting scheme, see Schröder and Sweldens (1996) or Jansen and Oonincx (2005).

In this section we introduce a *complex-valued* lifting scheme for analysing irregularly sampled signals. The proposed lifting scheme can be thought of as a wavelet lifting analogue to the Fourier transform. An irregularly sampled signal is decomposed into a set of complex-valued wavelet (or detail) coefficients, representing the variation in the data as a function of location and wavelet scale (comparable to Fourier frequency).

In a nutshell, the scheme can be conceptualised in two branches: one branch of the transform provides the real-valued part of the detail coefficient and the second branch represents

the imaginary component. Hence by using two different (real-valued) lifting schemes, one obtains a complex-valued decomposition, akin to the dual-tree complex wavelet transform of Kingsbury (2001). However, our approach differs from that of Kingsbury (2001) in that it employs two lifting schemes linked through orthogonal prediction filters, rather than two separate DWTs. The new scheme is therefore able to extract information from signals via the two filters whilst also naturally coping with the irregularity of the observations. Our approach also differs fundamentally from the complex-valued lifting techniques currently in the literature (Abbas and Tran, 2006; Shui et al., 2003) through the particular filter construction we propose (Section 2.2) in conjunction with the lifting construction that removes 'one coefficient at a time' (Section 2.1). This allows us to embed adaptivity in our complex-valued multiscale setup, i.e. construct wavelet functions whose smoothness adjusts to the local properties of the signal.

In what follows we introduce the proposed scheme using an abstract choice of real and imaginary filters, and the subject of filter choice is deferred until Section 2.2, while an overcomplete version of the complex-valued lifting transform is introduced in Section 2.3.

2.1   The algorithm

Suppose a function $f(\cdot)$ is observed at a set of n *irregularly* spaced locations, $\underline{x} = (x_1, \ldots, x_n)$. The proposed lifting scheme aims to decompose the data collected over the irregularly sampled grid, $\{(x_i, f_i = f(x_i))\}_{i=1}^n$, into a set of R smooth coefficients and $(n-R)$ complex-valued detail coefficients, with R the desired resolution level. The quantity R is akin to the primary resolution level in classical wavelet transforms, see Hall and Patil (1996) for more details.

We propose to construct a new complex-valued transform that builds upon the LOCAAT paradigm of Jansen et al. (2001, 2009), shown to efficiently represent local signal features in the fields of nonparametric regression (Nunes et al., 2006; Knight and Nason, 2009) and spectral estimation (Knight et al., 2012). We shall therefore refer to our proposed algorithm under the acronym $\mathbb{C}$-LOCAAT.

Similar to the real-valued LOCAAT algorithm, $\mathbb{C}$-LOCAAT can be described by recursively applying three steps: *split, predict* and *update*, which we detail below. At the first stage (n) of the algorithm, the smooth coefficients are set as $c_{n,k} = f_k$, the set of indices of smooth coefficients is $S_n = \{1, \ldots, n\}$ and the set of indices of detail coefficients is $D_n = \emptyset$.

The (irregular) sampling is described using the distance between neighbouring observations, and at stage n we define the *span* of x_k as $s_{n,k} = \frac{x_{k+1} - x_{k-1}}{2}$. The sampling irregularity is intrinsically linked to the notion of wavelet scale, which in this context becomes continuous, as opposed to dyadic in the classical wavelet settings; this results in each coefficient having an associated scale across a continuum. This aspect will be discussed in detail following the introduction of the $\mathbb{C}$-LOCAAT algorithm.

In the *split* step, a point j_n to be lifted is chosen. Typically, points from the densest sampled regions are removed first, but other predefined removal choices are also possible (see Section 2.3). We shall often refer to the removal order as a *trajectory*.

In the *predict* step the set of neighbours (J_n) of the point j_n are identified and used to estimate the value of the function at the selected point j_n. In contrast to real-valued LOCAAT algorithms, this is achieved using *two* prediction schemes, each defined by its respective filters, $\mathbf{L}$ and $\mathbf{M}$. The filter $\mathbf{L}$ corresponds to estimation via regression over the neighbourhood, as is usual in LOCAAT. In order to extract further information from the signal, our proposal is to construct the second filter ($\mathbf{M}$) orthogonal on $\mathbf{L}$, to ensure that it exploits further local signal information to the filter $\mathbf{L}$. Section 2.2 discusses this in detail.

The prediction residuals from using the two filters are given by

$$\lambda_{j_n} = l_{j_n}^n c_{n,j_n} - \sum_{i \in J_n} l_i^n c_{n,i}, \tag{1}$$

$$\mu_{j_n} = m_{j_n}^n c_{n,j_n} - \sum_{i \in J_n} m_i^n c_{n,i}, \tag{2}$$

where $\{l_i^n\}_{i \in J_n \cup \{j_n\}}$ and $\{m_i^n\}_{i \in J_n \cup \{j_n\}}$ are the prediction weights associated with $\mathbf{L}$ and $\mathbf{M}$.

The complex-valued detail (wavelet) coefficient we propose is obtained by combining the two prediction residuals

$$d_{j_n} = \lambda_{j_n} + \mathrm{i}\,\mu_{j_n}. \tag{3}$$

In the *update* step, the smooth coefficients $\{c_{n,i}\}_{i \in J_n}$ and spans of the neighbours $\{s_{n,i}\}_{i \in J_n}$ are updated according to filter $\mathbf{L}$:

$$
\begin{aligned}
c_{n-1,i} &= c_{n,i} + b_i^n \lambda_{j_n}, \\
s_{n-1,i} &= s_{n,i} + l_i^n s_{n,j_n} \qquad\qquad \forall i \in J_n,
\end{aligned} \tag{4}
$$

where b_i^n are update weights. In practice, the update weights are chosen such that the mean of the series is preserved throughout the transform, thus preserving the characteristics of the

original series (Jansen et al., 2009). One such choice is to set $b_i^n = (s_{n,j_n} s_{n-1,i})/(\sum_{i \in J_n} s_{n-1,i}^2)$. The neighbours' spans update accounts for the modification to the sampling grid induced by removing one of the observations. Updating according to the **L** filter only ensures that there is a unique coarsening of the signal for both the real and imaginary parts of the transform.

The observation j_n is then removed from the set of smooth coefficients, hence after the first algorithm iteration, the index set of smooth and detail coefficients are $S_{n-1} = S_n \backslash \{j_n\}$ and $D_{n-1} = \{j_n\}$ respectively. The algorithm is then iterated until the desired primary resolution level R has been achieved. In practice, the choice of the primary level R in LOCAAT lifting schemes is not crucial provided it is sufficiently low (Jansen et al., 2009), with $R = 2$ recommended by Nunes et al. (2006).

After observations $j_n, j_{n-1}, \ldots, j_{R+1}$ have been removed, the function can be represented as a set of R smooth coefficients, $\{c_{r-1,i}\}_{i \in S_R}$, and $(n-R)$ detail coefficients, $\{d_k\}_{k \in D_R}$ ($D_R = \{j_n, ..., j_{R+1}\}$). As in classical wavelet decompositions, the detail coefficients represent the high frequency components of $f(\cdot)$, whilst the smooth coefficients capture the low frequency content in the data.

The lifting scheme can be easily inverted by recursively 'undoing' the update, predict and split steps described above for the first filter. Specifically, the update step is first inverted: $c_{n,i} = c_{n-1,i} - b_i^n \lambda_{j_n}$, $\forall i \in J_n$, then the predict step is inverted by

$$c_{n,j_n} = \frac{\lambda_{j_n} - \sum_{i \in J_n} l_i^n c_{n,i}}{l_{j_n}^n} \qquad \text{or} \qquad (5)$$

$$c_{n,j_n} = \frac{\mu_{j_n} - \sum_{i \in J_n} m_i^n c_{n,i}}{m_{j_n}^n}. \qquad (6)$$

Undoing either predict (5) or (6) step is sufficient for inversion. As for real-valued lifting, inversion can also be performed via matrix calculations due to the transform linearity. However, using (5) for inversion is generally computationally faster, especially for large n.

Wavelet lifting scales. The notion of wavelet scale in this context becomes continuous and is intrinsically linked to the data sampling structure and trajectory (removal order) choice. Denote the lifting analogue of the classical wavelet scale for a detail coefficient d_{j_k} by $\alpha_{j_k} = \log_2(s_{k,j_k})$, with low α-values corresponding to fine scales. In order to give lifting scales a similar interpretation to the classical notion of dyadic wavelet scale, we group wavelet functions of similar α-scales into discrete artificial levels $\{\ell_i\}_{i=1}^{J^*}$, as proposed by Jansen et al.

6

(2009), for a chosen J^*. The further use of artificial scales is discussed in Sections 2.3 and 3 (under the spectral estimation context) and in Appendix B (under the nonparametric regression context). Note that the usage of the same lifting trajectory for the two lifting branches (coupled with the one filter update) ensures that our proposed lifting transform generates a common scale for both real and imaginary parts. In other words, at each stage of the algorithm there is just one set of smooth coefficients associated to a unique set of scales.
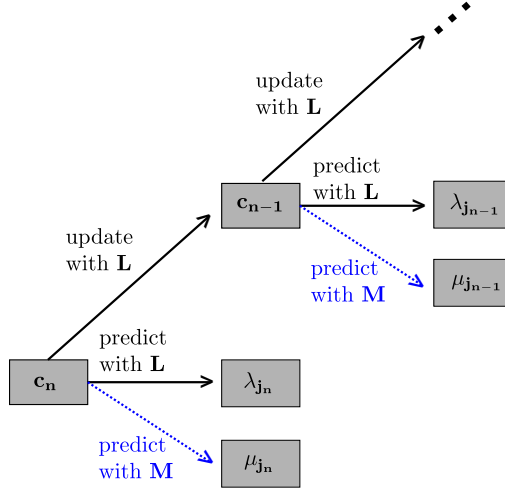

Figure 1: The complex-valued lifting scheme ($\mathbb{C}$-LOCAAT). Solid lines correspond to the steps of the standard LOCAAT lifting scheme whereas dotted lines indicate the extra prediction step required for the complex-valued scheme. After $(n-R)$ applications, the function can be represented as a set of R smooth coefficients $\{c_{r-1,i}\}_{i \in S_{n-R}}$ and $(n-R)$ detail coefficients $\{\lambda_{j_k} + i\mu_{j_k}\}_{k \in D_{n-R}}$, each associated with a particular scale $\{\alpha_{j_k}\}_{k \in D_{n-R}}$.

2.2 Filter construction

The proposed complex-valued lifting transform is illustrated schematically in Figure 1 in terms of two general prediction filters $\mathbf{L}$ and $\mathbf{M}$. As already explained, we construct the second filter ($\mathbf{M}$) orthogonal on $\mathbf{L}$, thus ensure different signal content extraction.

For clarity of exposition, let us consider a LOCAAT scheme with a prediction step based upon two neighbours in a symmetrical configuration. The regression over the neighbourhood generates prediction weights for the two neighbours, let us denote them by l_1 and l_3 (see equation (1)); this prediction step can also be viewed as using a three-tap prediction filter

7

($\mathbf{L}$) of the form $(l_1, 1, l_3)$, which depends on the sampling of the observations $\underline{x} = (x_1, \ldots, x_n)$ (Nunes et al., 2006). We determine the unique (up to proportionality) three-tap filter $\mathbf{M}$ that is orthogonal on $\mathbf{L}$ and ensures at least one vanishing moment. Hence we can express the set of filter pairs as having the form

$$
\begin{aligned}
\mathbf{L} &= (l_1, 1, l_3), \quad l_1, l_3 > 0 \\
\mathbf{M} &= (m_1, m_2, m_3),
\end{aligned}
$$

and $l_1 m_1 + m_2 + l_3 m_3 = 0$ (i.e. $\mathbf{L} \cdot \mathbf{M} = 0$) and $l_1 + l_3 = 1$, $m_1 + m_3 = m_2$ (i.e. ensure one vanishing moment). The solution to these constraints can be parameterised as $\mathbf{M} = (-\frac{1+l_3}{1+l_1} m, \frac{l_1 - l_3}{1+l_1} m, m)$. The proportionality constant can be determined by bringing both filters $\mathbf{L}$ and $\mathbf{M}$ to the same scale through $\|\mathbf{L}\| = \|\mathbf{M}\|$, which yields $m = \frac{l_1 + 1}{\sqrt{3}}$. Hence the solution can be succinctly written as $\mathbf{M} = (Am, (1 + A)m, m)$ with $A = \frac{l_1 - 2}{l_1 + 1}$ and $m = \frac{l_1 + 1}{\sqrt{3}}$. This particular example of the lead filter $\mathbf{L}$ represents a prediction scheme using linear regression with two neighbours in a symmetrical configuration. This is a choice that has proved to be successful both for (real-valued) nonparametric regression (Nunes et al., 2006; Knight and Nason, 2009) and for (real-valued) spectral estimation (Knight et al., 2012).

Since $\mathbf{L}$ can be viewed as a prediction filter for a real-valued LOCAAT scheme, we can also employ the *adaptive* prediction filter choice of Nunes et al. (2006) in our proposed construction. The 'best' local regression (order and neighbourhood) is chosen at each predict step, subject to yielding minimising the detail coefficients. Consequently, we obtain an *adaptive complex-valued lifting transform*, with the highly desirable flexibility of being able to adapt to the local characteristics of the data – see Appendix B in the supplementary material for an illustration of this adaptiveness in the nonparametric regression setting.

The orthogonality of the two filters $\mathbf{M}$ and $\mathbf{L}$ also mirrors the attractive properties of Fourier sinusoids, hence this choice results in an interpretable quantification of phase, which shall further be exploited according to the context—by phase alteration when denoising real-valued signals, or by ensuring phase preservation in the context of spectral estimation.

A further insight and justification of the proposed filter choice is provided in Appendix C in the context of coherence and phase estimation.

2.3   The nondecimated complex-valued lifting transform

In the classical wavelet literature, the nondecimated wavelet transform (NDWT) (Nason and Silverman, 1995) has properties that make it a better choice than the discrete wavelet transform (DWT) for certain classes of problems, see e.g. Percival and Walden (2006). The concept is akin to basis averaging, and has delivered successful results in both nonparametric regression and spectral estimation problems, not only in the classical wavelet setting (NDWT) but also for irregularly spaced data through the nondecimated lifting transform (NLT) (Knight and Nason, 2009; Knight et al., 2012).

In this section, we also exploit the benefits of this nondecimation paradigm for irregularly sampled data and to this end, we shall introduce the *complex-valued nondecimated lifting transform* ($\mathbb{C}$NLT). However, note that our use of the term 'nondecimation' differs from the classical NDWT. Specifically, due to the irregular sampling structure, nondecimation cannot be performed via decomposing shifts of input data without data interpolation.

Although similar in spirit to the NLT, our transform hinges on the proposed complex-valued lifting scheme (Section 2.1) and therefore yields an overcomplete complex-valued data representation, extracting additional signal information. In particular, the $\mathbb{C}$NLT algorithm results in a wavelet transform that yields (complex-valued) wavelet coefficients at each grid point (x) and at multiple scales (α).

Next we shall describe our proposed univariate and bivariate $\mathbb{C}$NLT techniques. We shall show that in the nonparametric regression setting, our univariate proposal significantly outperforms current wavelet and non-wavelet denoising techniques (see Section 4 and Appendix B), while its bivariate extension allows for estimation of the dependence between pairs of series (see Section 3).

2.3.1   Univariate $\mathbb{C}$NLT

So far, the proposed complex-valued lifting scheme decomposes the original signal $\{(x_i, f_i = f(x_i))\}_{i=1}^n$ into a set of R smooth coefficients and $(n-R)$ complex detail (wavelet) coefficients, with each detail coefficient d_{j_k} corresponding to exactly *one* scale α_{j_k}.

We now aim to construct a new scheme that transforms the original signal into a collection of smooth and detail coefficients, with each x-location associated to a collection of several

wavelet coefficients spread over all scales, rather than just one. The key to our proposal is to note that if an observation is removed early in the LOCAAT algorithm, its associated detail coefficient has a fine scale; conversely, if a point is removed later in the algorithm, it is associated with a larger scale.

We therefore propose to repeatedly apply $\mathbb{C}$-LOCAAT using randomly drawn trajectories, T_p for $p = 1, ..., P$, where each removal order T_p is generated by sampling $(n - R)$ locations without replacement from $(x_1, \ldots, x_n)$; we refer to this algorithm as $\mathbb{C}$NLT.

Following this procedure, a set of P detail coefficients $\{d_{x_k}^p\}_{p=1}^P$ is generated at each location x_k, where $d_{x_k}^p$ denotes the wavelet coefficient at location x_k obtained using $\mathbb{C}$-LOCAAT with trajectory T_p. At any given location x_k, the set of P detail coefficients will be associated with different scales, $\{\alpha_{x_k}^p\}_{p=1}^P$; note that this differs from the classical NDWT which produces exactly one detail coefficient at each location and dyadic scale.

Similar to the NLT, the number of trajectories P should be 'large enough' to ensure that an ample number of coefficients is produced at as many scales and locations as possible, subject to computational constraints (Knight and Nason, 2009; Knight et al., 2012).

2.3.2 Bivariate $\mathbb{C}$NLT

We now consider the extension of $\mathbb{C}$NLT to the analysis of bivariate series.

Same irregular grid. Let us first assume we have observations $\{(x_i, f_i^1, f_i^2)\}_{i=1}^n$ on two functions f^1 and f^2, measured on the *same* x-grid. Apply the univariate $\mathbb{C}$NLT (Section 2.3.1) to each signal, using the same set of trajectories $\{T_p\}_{p=1}^P$ for both series.

The identical sampling grids results in an exact correspondence between the coefficients of each series, i.e. for each coefficient of the first series there is a coefficient of the second series at exactly the same location and scale (see Figure 2a). In other words, after application of the $\mathbb{C}$NLT to both series, for each time point, x_k, we obtain two sets of complex-valued detail coefficients $\{d_{x_k}^{1,p}\}_{p=1}^P$ and $\{d_{x_k}^{2,p}\}_{p=1}^P$.

Different irregular grids. Let us now assume we have the data $\{(x_i^1, x_i^2, f_i^1, f_i^2)\}_{i=1}^n$ on two functions f^1 and f^2, measured on the *different* x-grids.

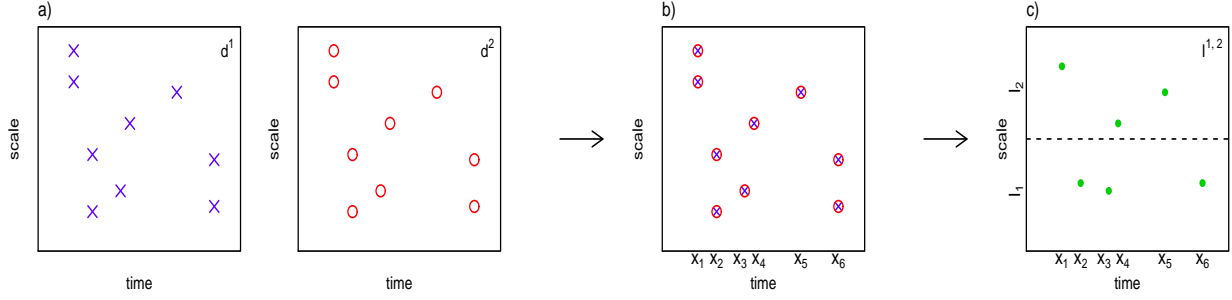As the scale associated with each detail coefficient is determined by the trajectory choice,

10

Figure 2: Construction of bivariate $\mathbb{C}$NLT transform for time series observed on the same sampling grid (x refers to time here): a) univariate $\mathbb{C}$NLT is applied using the same set of trajectories for both series and yields two sets of detail coefficients $\{d_{x_k}^{1,p}\}_{p,k}$ and $\{d_{x_k}^{2,p}\}_{p,k}$; b) the $\mathbb{C}$NLT transform consists of combinations of coefficients from each series; c) the detail coefficients are averaged within each scale.

we partition the x-grid into a set of *artificial* x-intervals $\{x^{(j)}\}_{j=1}^{T^*}$, where T^* is chosen to provide the desired resolution level on the x-axis. As illustrated in Figure 3, the result can be visualised in terms of forming a grid over the area of the resulting detail coefficients.

Formally, for each artificial x-interval $\{x^{(j)}\}_{j=1}^{T^*}$ and artificial scale $\{\ell^i\}_{i=1}^{J^*}$, the set of detail coefficients for each grid square (using trajectories $\{T_p\}_{p=1}^P$) is given by

$$D_{x^{(j)}}^1(\ell^i) = G_m\big(d_{x_k^1}^{1,p} | \alpha_{x_k^1}^{1,p} \in \ell^i, x_k^1 \in x^{(j)}\big) \tag{7}$$

$$D_{x^{(j)}}^2(\ell^i) = G_m\big(d_{x_k^2}^{2,p} | \alpha_{x_k^2}^{2,p} \in \ell^i, x_k^2 \in x^{(j)}\big), \tag{8}$$

where $d_{x_k^1}^{1,p} = \lambda_{x_k^1}^{1,p} + \mathrm{i}\,\mu_{x_k^1}^{1,p}$ and $d_{x_k^2}^{2,p} = \lambda_{x_k^2}^{2,p} + \mathrm{i}\,\mu_{x_k^2}^{2,p}$ are the complex-valued wavelet coefficients from f^1 and f^2, and G_m is a random sampling procedure selecting $m_{i,j} = \min(\#(d^1), \#(d^2))$ coefficients. Recall that $\alpha_{x_k^1}^{1,p}$ and $\alpha_{x_k^2}^{2,p}$ represent the scales ($\log_2$ of span) associated to the coefficients $d_{x_k^1}^{1,p}$ and $d_{x_k^2}^{2,p}$. Thus for each artificial x-interval and scale, we obtain the same number of detail coefficients (although the exact coordinates of the coefficients may differ).

We term these constructions as the *bivariate complex nondecimated lifting transform* (bivariate $\mathbb{C}$NLT) on the same/different grid(s), as appropriate. Section 3 will discuss applications where the proposed bivariate $\mathbb{C}$NLT construction provides a framework for estimation of the dependence between pairs of series.
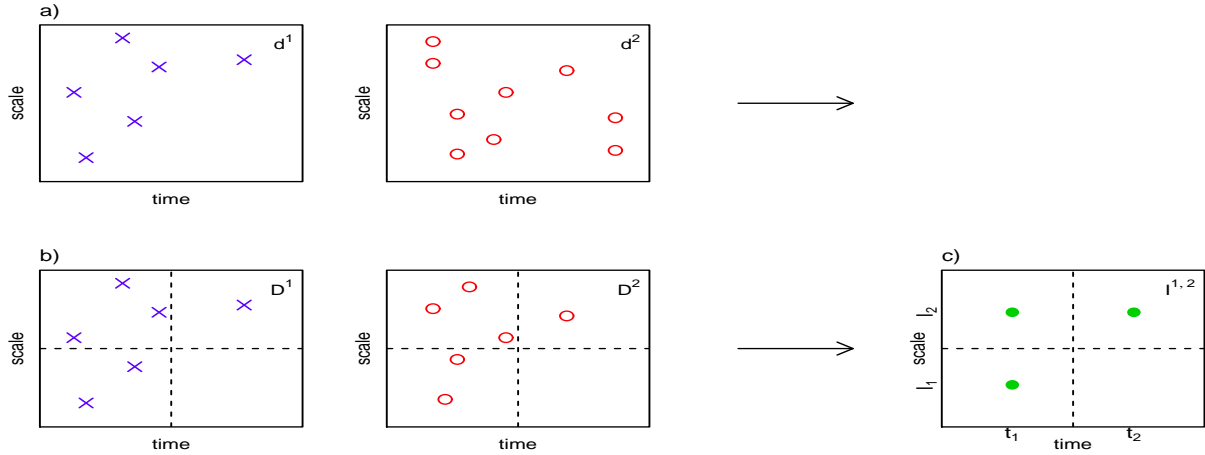
11

Figure 3: Construction of bivariate ℂNLT transform for time series observed on different sampling grids (x refers to time here): a) each series is lifted individually as described in Section 2.3; b) the sets of coefficients in each grid square. The coefficients are sampled so that there is the same number in the grid square of each series; c) the coefficients of each series are combined to form the appropriate bivariate quantities, producing one coefficient to represent each grid square.

3 Complex lifting analysis of irregularly sampled time series

Spectral analysis is an important tool in describing content in time series data, complementary to time domain analysis. In particular, the Fourier spectrum allows a decomposition in terms of sinusoidal components at different frequencies, giving a description of the strength of periodic behaviour within the series. Such traditional methods are based on the assumption of second-order stationarity, although extensions to deal with non-stationarity exist, such as the short-time Fourier transform (STFT, Allen (1977); Jacobsen and Lyons (2003)) or more sophisticated time-frequency analysis methods (e.g. locally stationary time series, Nason et al. (2000); SLEX, Ombao et al. (2002)). Similarly, *cross-spectral* analysis of multivariate time series can be used to describe and study the interrelationships between many variables of interest observed simultaneously over time, see Reinsel (2003) or Lütkepohl (2005) for comprehensive introductions to the area, or Park et al. (2014) for a multivariate locally

12

stationary wavelet approach.

This work aims to deal with a further additional challenge, that of irregular sampling. Irregularly sampled time series arise in many scientific applications, e.g. finance (Engle, 2000; Gençay et al., 2001), astronomy (Bos et al., 2002; Broerson, 2008) and environmental science (Witt and Schumann, 2005; Wolff, 2005) to name just a few. Many applications deal with the sampling irregularity either by means of a time-frequency Lomb-Scargle approach under the assumption of time series stationarity (Vaníček, 1971; Lomb, 1976; Scargle, 1982), or process the data prior to analysis, restoring it to a regular grid then suitable for analysis by standard methods, see for example Erdogan et al. (2004) or Broerson (2008). Although it is convenient to work within a regularly spaced time series setting, a typical result will amount to signal smoothing, leading to information loss at high frequencies and estimation bias (Frick et al., 1998; Rehfeld et al., 2011).

Many time series observed in practice will exhibit (second-order) nonstationary behaviour as well as being irregularly sampled. Although the literature does currently offer (albeit few) options for the analysis of irregularly sampled nonstationary series (see e.g. Foster (1996); Frick et al. (1998); Knight et al. (2012)), there is no well established method for estimating the dependence between pairs of such signals. In the next section, we propose to describe the local frequency content of irregularly sampled time series by making use of the proposed complex-valued lifting scheme and introducing a complex-valued cross-periodogram and associated measures.

3.1   The complex lifting periodogram

Recall that the $\mathbb{C}$NLT provides a set of detail coefficients and associated scales $\{d_{x_k}^p, \alpha_{x_k}^p\}_{p=1}^P$, where the scale associated with each detail coefficient $\alpha_{x_k}^p$ is a continuous quantity. In a spirit similar to that of Knight et al. (2012), this information will allow a time-scale decomposition (typically termed the (wavelet) periodogram) of the variability in the data, with the crucial difference that the wavelets coefficients are now complex-valued and therefore contain more information. In constructing the periodogram, we use a set of discrete artificial scales, $\{\ell^i\}_{i=1}^{J^*}$, which partitions the range of the continuous lifting scales $\{\alpha_{x_k}^p\}$ for all p and k, with J^* chosen to provide a desired periodogram 'granularity'. Each scale $\alpha_{x_k}^p$ will fall into one unique level ℓ^i for each p and observation x_k; let $P_{i,k} = \{p : \alpha_{x_k}^p \in \ell^i\}$ denote the set of

trajectories such that x_k is associated with a scale in the set ℓ^i, and $n_{i,k} = |P_{i,k}|$ denote the size of the set. For each time point x_k, $k = 1, \ldots, n$ and artificial scale ℓ^i, $i = 1, \ldots, J^*$, we introduce the *complex lifting periodogram* (also referred to in text as $\mathbb{C}$NLT periodogram)

$$I_{x_k}(\ell^i) = \frac{1}{n_{i,k}} \sum_{p \in P_{i,k}} |d_{x_k}^p|^2 = \frac{1}{n_{i,k}} \sum_{p \in P_{i,k}} (\lambda_{x_k}^p)^2 + \frac{1}{n_{i,k}} \sum_{p \in P_{i,k}} (\mu_{x_k}^p)^2,$$

where $|\cdot|$ denotes the complex modulus.

3.2   The complex lifting cross-periodogram

Similar to other complex wavelet transforms (Portilla and Simoncelli, 2000; Selesnick et al., 2005), the complex-valued nature of the bivariate $\mathbb{C}$NLT coefficients (see Section 2.3.2) provides both local phase and spectral information. In order to estimate the dependence between pairs of time series, we first define the *complex lifting cross-periodogram*, the cross-spectral analogue of the periodogram. As in Section 2.3.2, our discussion will be split based on whether the data has been sampled over the same or different grids.

Bivariate time series observed on the same grid.   For each time point x_k, $k = 1, \ldots, n$ and artificial scale ℓ^i, $i = 1, \ldots, J^*$, define the complex lifting cross-periodogram (also referred to as $\mathbb{C}$NLT cross-periodogram) for series observed on the same grid as

$$I_{x_k}^{(1,2)}(\ell^i) = \frac{1}{n_{i,k}} \sum_{p \in P_{i,k}} d_{x_k}^{1,p} \overline{d_{x_k}^{2,p}}, \tag{9}$$

where $d_{x_k}^{1,p} = \lambda_{x_k}^{1,p} + \mathrm{i}\,\mu_{x_k}^{1,p}$ and $d_{x_k}^{2,p} = \lambda_{x_k}^{2,p} + \mathrm{i}\,\mu_{x_k}^{2,p}$ are the detail coefficients from f^1 and f^2. The $\mathbb{C}$NLT cross-periodogram consists of combinations of coefficients from each series and provides information about the relationship between the signals. Note that unlike the $\mathbb{C}$NLT periodogram, the cross-periodogram is complex-valued.

Similar to classical Fourier cross-spectrum methodology (see e.g. Priestley (1983)), the $\mathbb{C}$NLT cross-periodogram can be separated into its real and imaginary parts to define the $\mathbb{C}$*NLT co-periodogram* and the $\mathbb{C}$*NLT quadrature periodogram*, respectively resulting in

$$c_{x_k}(\ell^i) = \frac{1}{n_{i,k}} \sum_{p \in P_{i,k}} \lambda_{x_k}^{1,p} \lambda_{x_k}^{2,p} + \frac{1}{n_{i,k}} \sum_{p \in P_{i,k}} \mu_{x_k}^{1,p} \mu_{x_k}^{2,p},$$

$$q_{x_k}(\ell^i) = \frac{1}{n_{i,k}} \sum_{p \in P_{i,k}} \mu_{x_k}^{1,p} \lambda_{x_k}^{2,p} - \frac{1}{n_{i,k}} \sum_{p \in P_{i,k}} \lambda_{x_k}^{1,p} \mu_{x_k}^{2,p}.$$

These quantities, together with the individual lifting spectra of each process, can be used to calculate the measures of *phase* and *coherence* between the two series f^1 and f^2:

$$\phi_{x_k}(\ell^i) = \tan^{-1}\left(\frac{-q_{x_k}(\ell^i)}{c_{x_k}(\ell^i)}\right), \tag{10}$$

$$\rho_{x_k}(\ell^i) = \frac{\sqrt{c_{x_k}(\ell^i)^2 + q_{x_k}(\ell^i)^2}}{\sqrt{I_{x_k}^{(1)}(\ell^i) I_{x_k}^{(2)}(\ell^i)}}. \tag{11}$$

The $\mathbb{C}$NLT cross-periodogram provides a measure of the dependence between series, but its magnitude is affected by the individual $\mathbb{C}$NLT periodograms of the signals. Hence as in the regularly sampled setting, it is preferable to normalise this quantity, providing a coherence measure that satisfies $0 \leq \rho_{x_k}(\ell^i) \leq 1$ (as in (11)). This is similar to the coherence measure for regularly sampled signals introduced in Sanderson et al. (2010). The $\mathbb{C}$NLT phase as defined in (10) provides an indication of any time lag between the signals. Several examples examining the coherence and phase between signal pairs are given in Section 3.3.

Bivariate time series observed on different grids. Closer to real data scenarios, we now consider time series that were sampled over different irregular grids, with one such real data example being discussed in Section 3.3.3. In order to obtain the cross-spectral quantities, we combine the appropriate sets of detail coefficients for each grid, corresponding to f^1 and f^2, i.e. $D_{x^{(j)}}^1(\ell^i)$ and $D_{x^{(j)}}^2(\ell^i)$ introduced in equations (7) and (8). For each artificial time period, $x^{(j)}$, $j = 1, \ldots, T^*$ and artificial scale ℓ^i, $i = 1, \ldots, J^*$, we define the complex lifting cross-periodogram for series observed on different irregular grids as

$$I_{x^{(j)}}^{(1,2)}(\ell^i) = \frac{1}{n_{i,j}} \sum_{s=1}^{n_{i,j}} \text{order}\{D_{x^{(j)}}^1(\ell^i)\}_s \, \text{order}\{\overline{D_{x^{(j)}}^2(\ell^i)}\}_s, \tag{12}$$

where $n_{i,j}$ is the number of pairs in the grid square defined at time $x^{(j)}$ and scale ℓ^i, and order$\{D\}_s$ indicates the sth time-ordered detail.

If the sampling schemes coincide for the two series ($\{x_k^1\}_k \equiv \{x_k^2\}_k$) and the same trajectories are used to generate the details $\{d_{x_k}^{1,p}\}_{p,k}$, respectively $\{d_{x_k}^{2,p}\}_{p,k}$, then equations (9) and (12) coincide, except for the quantities being also averaged over the defined artificial time period. The co- and quadrature periodograms may be obtained in the same fashion as above, and subsequently used to yield the lifting phase and coherence in this setting.

15

Figures 2 and 3 provide a visual representation for the complex lifting cross-periodogram construction under the assumption of the same, respectively different sampling grids. We now make some remarks about the proposed periodogram constructions.

Scale interpretation. The relationship between artificial scale (ℓ^i) and classical Fourier frequency can be described in terms of the scale which maximises the coherence for a Fourier wave of period T. Defining $\rho(\ell^i) = \frac{1}{n} \sum_{k=1}^{n} \rho_{x_k}(\ell^i)$, the design of the filters outlined in Section 2.2 is such that $\ell^i = \text{argmax}_{j \in \{1, \ldots, J^*\}} \rho(\ell^j) = T/3$.

We emphasise that this relationship is dictated by the choice of filter pairs: the $\mathbb{C}$NLT periodogram and co-periodogram (as defined above) are composed of the sum of the wavelet coefficients from the two schemes, while the quadrature periodogram contains products of the coefficients. Hence to ensure that the resulting estimates are interpretable, the two filters are specified so that combinations of coefficients (either through multiplication or summation) provide the same scale-frequency relationship (see Sanderson (2010), Sections 5.3 and 6.2.1). The provided mapping between wavelet lifting scale and Fourier frequency can be used to compare our results to those of classical Fourier-based methods (see Section 3.3 next).

Periodogram smoothing over time. As is customary, the $\mathbb{C}$NLT periodogram will be smoothed over time using simple moving average smoothing, i.e. we compute $\tilde{I}_{x_k}(\ell^i) = \frac{1}{\#(M_k^i)} \sum_{j \in M_k^i} I_{x_j}(\ell^i)$, where $M_k^i = \{j : x_k - M^i < x_j \le x_k + M^i\}$ and M^i denotes the width of the averaging window, permitted to take different values for each scale, l^i.

3.3 Examples

We now illustrate the proposed methodology by application to both simulated and real irregular time series. The results were produced in the R statistical computing environment (R Core Team, 2013), using modifications to the code from the *adlift* package (Nunes and Knight, 2012) and the *nlt* package (Knight and Nunes, 2012).

3.3.1 Simulated data

Signals sampled on the same irregular sampling grid. In this example, the methods of Section 3.2 are applied to bivariate series observed on the same sampling grid:

$\{(x_k, f_k^1, f_k^2)\}_{k=1}^{200}$, where

$$f_k^1 = \sin\left(\frac{2\pi x_k}{10}\right) + \sin\left(\frac{2\pi x_k}{30}\right) + \sin\left(\frac{2\pi x_k}{70}\right) + \zeta_k^1,$$

$$f_k^2 = \sin\left(\frac{2\pi(x_k - \tau)}{30}\right) + \zeta_k^2,$$

where $\tau = 0$ for $x_k < 200$ and $\tau = 6$ for $x_k \geq 200$, and the quantities ζ_k^1 and ζ_k^2 are independent, identically distributed Gaussian variables with mean zero and variance 0.2^2. The observations are irregularly sampled such that $(x_{k+1} - x_k) \in \{n/10 : n = 10, 11, \ldots, 30\}$ and $\frac{1}{(n-1)} \sum_{k=1}^{n-1}(x_{k+1} - x_k) = 2$.

Estimates for coherence and phase are computed using the complex-valued lifting scheme using a sample of $P = 1500$ randomly sampled trajectories, discretising using $J^* = 20$ artificial scales and smoothing over time using a window of width $M^i = 60, \forall\ i$. The coherence estimate (Figure 4, right) provides a clear visualisation of the dependence between the two series, with a peak occurring at scale $\log_2(30/3) = 3.3$ (equivalent to a Fourier period of 30). The time lag that is introduced halfway through the second signal is also clearly captured by the phase estimate (Figure 5, left), which is approximately zero for the first half of the series, then shows a marked increase for the second half.
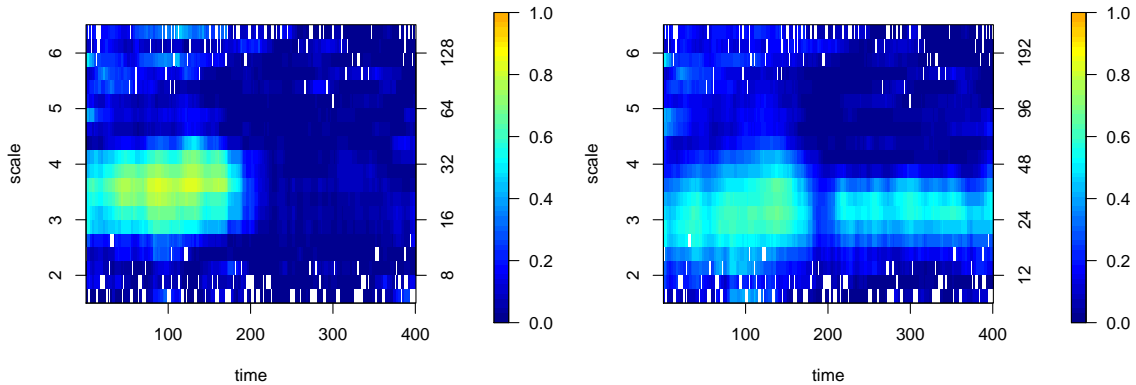

Figure 4: Coherence estimation for data observed on the same irregular sampling grid: using the real-valued bivariate lifting scheme (left); using the complex-valued lifting scheme (right). Scale gets coarser from bottom upwards.

For comparison, the estimated coherence using a real-valued bivariate scheme (Sanderson, 2010) is also reported (Figure 4, left). It is interesting to note that although this method
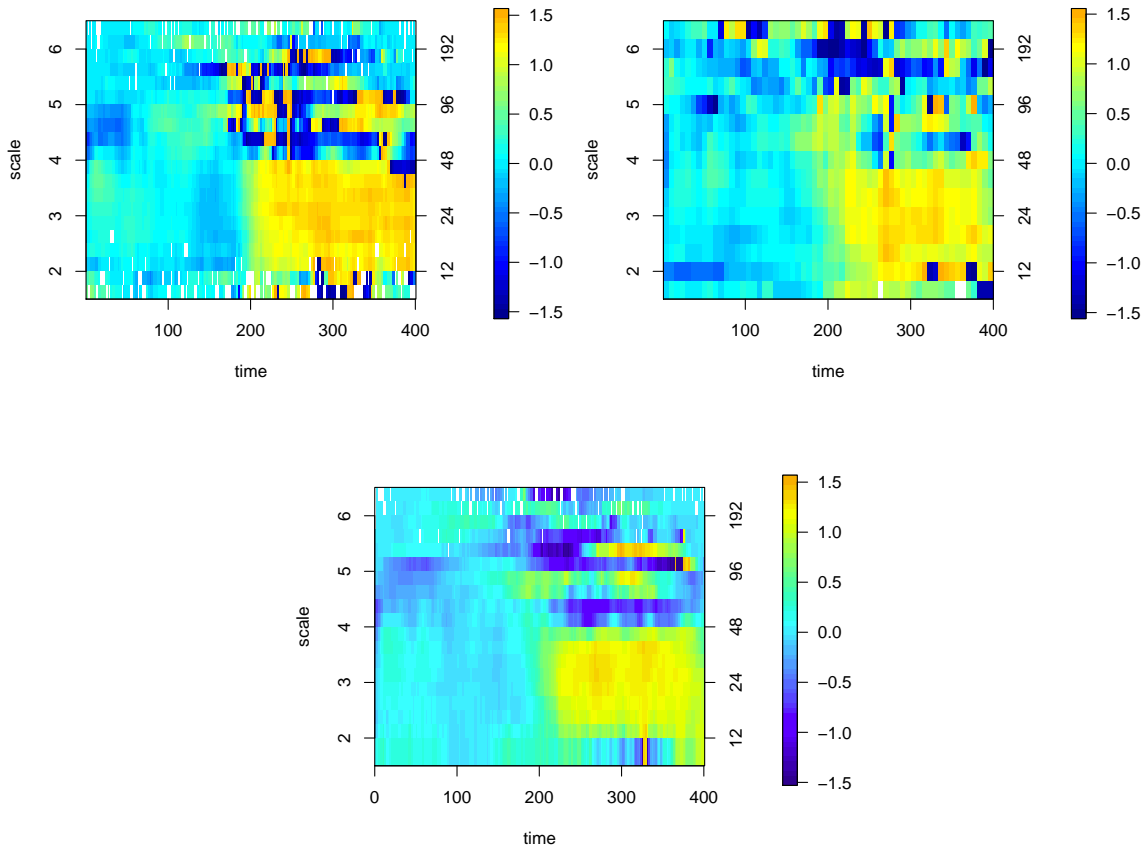
17

Figure 5: Phase estimation using the complex-valued lifting scheme: data observed on the same irregular sampling grid (left); data observed on different irregular sampling grids (right); data observed on the same regular grid (bottom). Scale gets coarser from bottom upwards.

also clearly estimates a dependence for the first half of the series, it does not continue to detect it following the time delay. This again emphasises the advantage of using a second filter, present in the complex-valued lifting transform.

Signals sampled on different irregular sampling grids. The methods described in Section 3.2 are now demonstrated by revisiting the same simulated data example, but with the two series observed on different irregularly spaced sampling grids: $\{(x_k^1, x_k^2, f_k^1, f_k^2)\}_{k=1}^{200}$. Aside from the sampling, the series satisfy the same properties as previously described.

The estimates were obtained using a discretisation of $J^* = 15$ artificial scales and $T^* = 60$ artificial time points, while a smoothing window of width $M^i = 60$ was applied at all scales

as in the previous example. The resulting estimated coherence and phase are shown in Figure 6, respectively Figure 5, right. It is interesting to note that while estimates broadly agree with those corresponding to sampling using the same (irregular) grid (Figure 4 and Figure 5, left), the price to pay for the different sampling schemes is the reduced clarity of the estimator. This is point is further reinforced by the phase estimate corresponding to a regular sampling situation, see Figure 5, bottom.
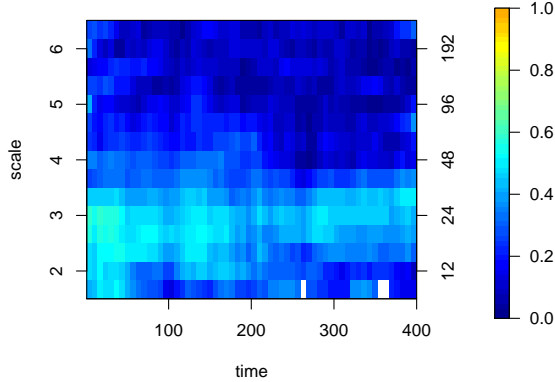

Figure 6: Coherence estimation for data observed on different irregular sampling grids. Scale gets coarser from bottom upwards.

Coherence and phase analysis comparison with Fourier-based methods. For comparison with established Fourier-based techniques, we also performed coherence analysis of stationary, regularly sampled vector autoregressive (VAR) processes, as well as phase analysis of the signals described above. For regularly sampled stationary processes, we compared our estimates to the well-behaved Fourier estimates, while in the presence of sampling irregularity/nonstationarity, we compared our method to the short-time Fourier transform (STFT) and the Lomb-Scargle method. For brevity, we do not include the coherence and phase comparison plots here, but they can be found in Appendix A of the supplementary material.

Specifically, in the supplementary material we illustrate the coherence estimates obtained through both a classical Fourier-based approach and our lifting-based method on two bivariate VAR processes. The resulting estimates agree very well, with the lifting-based estimate

displaying a slight depreciation when compared to the well-behaved Fourier estimates, suited for regular sampling and stationary process behaviour. However, in general if the data is believed to be amenable to be analysed with standard methodology, Fourier-based estimation should be preferred to the proposed method which was specifically designed to offer a solution for the challenging situations that include irregular sampling.

As already highlighted, traditional methods do not readily handle data that feature both potential nonstationarities and irregular sampling, thus STFT required further intervention while the Lomb-Scargle method failed to account for nonstationarity. Thus in order to obtain the desired phase analysis, we mapped the irregular data to a regular grid (by e.g. interpolation) and then used STFT in order to capture the nonstationary time-frequency content of the data. The Lomb-Scargle analysis naturally dealt with the sampling irregularity, but assumed stationarity and therefore it did not provide time-localisation information. The phase estimation plots of the STFT method exhibit little resolution in time or frequency, possibly due to the spectral blurring induced by the overlapping windows in the STFT as noted in Shumway and Stoffer (2013). Furthermore, for signals sampled over different irregular grids, the method creates additional blurring in the phase plot. By contrast, the Lomb-Scargle method is able to deal naturally with the irregular sampling structure of the signals, but it does not contain any time-phase information. In addition, there is no marked distinction in frequency where the phase is large, unlike for that of our complex lifting method (see Figure 5). These features yet again highlight the appeal of our technique.

3.3.2 Simulated data with varying time delay

The next example explores the effect of increasing the time delay between two signals. For each value of $\tau = 1, \ldots, 15$, the series $\{(x_k, f_k^1, f_k^2)\}_{k=1}^{200}$ are simulated following

$$
\begin{aligned}
f_k^1 &= \sin\left(\frac{2\pi x_k}{30}\right) + \zeta_k^1, \\
f_k^2 &= \sin\left(\frac{2\pi(x_k - \tau)}{30}\right) + \zeta_k^2,
\end{aligned}
$$

where $(x_{k+1} - x_k) \in \{n/10 : n = 10, 11, \ldots, 30\}$ and $\frac{1}{(n-1)}\sum_{k=1}^{n-1}(x_{k+1} - x_k) = 2$, ζ_k^1 and ζ_k^2 are independent, identically distributed Gaussian variables with mean zero, variance 0.2^2.

Just as in the classical (Fourier) analysis, it is interesting to inspect the coherence and phase across frequencies (here, scales) in order to relate the common behaviour of the two

series and possible time delays, respectively. The estimated coherence and phase corresponding to the increasing $\tau = 1, \ldots, 15$ are shown in Figure 7. To give an overall sense of the coherence and phase magnitude over time, the estimates are averaged over the full time range to give $\rho(\ell^i) = \frac{1}{200} \sum_{k=1}^{200} \rho_{x_k}(\ell^i)$. We used $P = 750$ randomly sampled trajectories and discretised using $J^* = 20$ artificial scales.

When $\tau = 0$, the coherence is 1 and the phase is 0. For $\tau \neq 0$ the coherence is greatest at a scale of $\log_2(30/3)$, corresponding to the period of variation ($T = 30$) in the data. The coherence intensity and response over scale are affected by the magnitude of the time delay. The coherence is lowest at time delays around 7.5 ($T/4$), and at these shifts the peak at scale $\log_2(30/3)$ is also more pronounced. At $\tau = 15$ ($T/2$) the signals are sign reversed versions of each other and, again, the observed coherence is 1 at all scales. The phase is also greatest at scale $\log_2(30/3)$. The phase response varies as a function of time delay and alternates between positive and negative values, with $|\phi(\ell^i)|$ maximised at $\ell^i = T/4$. This is displayed in Figure 8 which shows the estimated phase at scale $\log_2(30/3)$ as a function of time delay.

For completeness, we also provide a direct comparison with classical Fourier coherence and phase estimation when the signals are regularly sampled (see Figure 9). Whilst the overall behaviour is similar for both the classical and $\mathbb{C}$NLT methods, the Fourier method displays less variability across coherence estimates with the changing time delay (Figure 9, left), as well as more localised phase-frequency information (Figure 9, right). However, in general, note that if the data is believed to be amenable to be analysed with standard methodology, this should be preferred to the proposed $\mathbb{C}$NLT method which was specifically designed to offer a solution for the challenging situations that include irregular sampling.

3.3.3 Financial time series

In this section we demonstrate the use of the proposed complex-valued lifting transform through an application to financial data consisting of prices of all trades on 1 March 2011 (in normal trading hours) for two IT companies, Baidu and Google, both traded on the NASDAQ stock exchange. Comparison of the two companies is of interest as the main product of both is a search engine, but they are based in different geographical regions.

Often several trades per second occur and in this case the last quoted value for each second is selected. Thus the finest sampling interval is one second, but as there are seconds
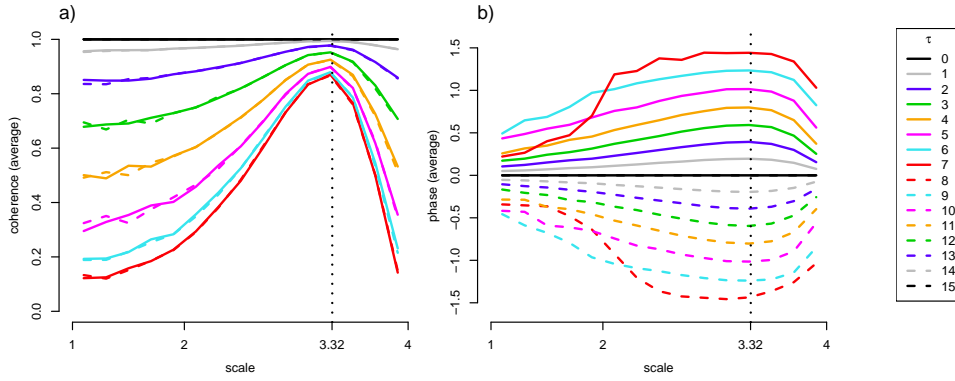
Figure 7: a) Coherence and b) Phase between f^1 and f^2 (Section 3.3.2) as a function of scale and $\tau \in \overline{0, 15}$. For $\tau \neq 0$ the coherence and (absolute) phase are greatest at scale $\log_2(30/3)$.
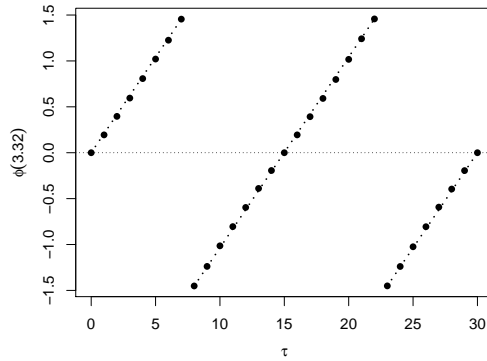

Figure 8: Estimated phase between f^1 and f^2 (Section 3.3.2) at scale $\log_2(30/3)$ (equivalent to a Fourier period of 30), as a function of τ.

with no trades, the time series are not equally spaced. For the analysis we consider the returns of each series– for Google, the series contains 7984 observations with an average sampling distance of 2.93 seconds and range 1 to 48; for Baidu, the series contains 6535 observations with an average sampling gap of 3.58 seconds and range 1 to 52.

The data was analysed using the methodology described in Section 3.2 using $J^* = 15$ artificial scales and $T^* = 390$ artificial time intervals (each time interval has a width of 60 seconds). The estimates were smoothed over time using a window width of $M^1 = 60$ minutes at the finest scale and increasing by a factor of 1.05, to provide a larger smoothing window for each subsequent scale. The coherence estimate is shown in Figure 10a) for scales up to 10.
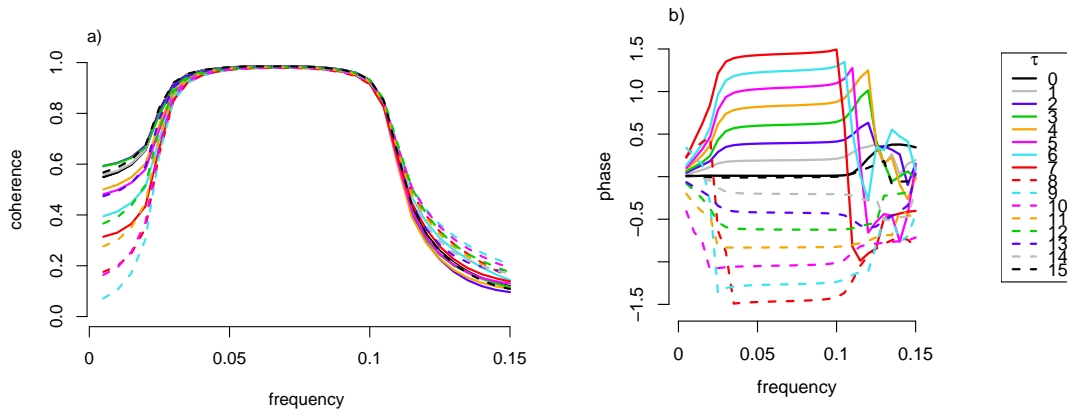
Figure 9: a) Coherence and b) Phase between f^1 and f^2 (Section 3.3.2) as a function of frequency and $\tau \in \overline{0, 15}$ using classical Fourier methods.

The main feature of the resulting coherence estimate is an increased coherence around scale 6, corresponding to a Fourier frequency of $T \approx 3$ minutes. The magnitude of the coherence at this scale is seen to be more pronounced towards the end of the day. There is also a period of higher coherence observed in the middle of the day, at low wavelet scales (corresponding to high frequency information).
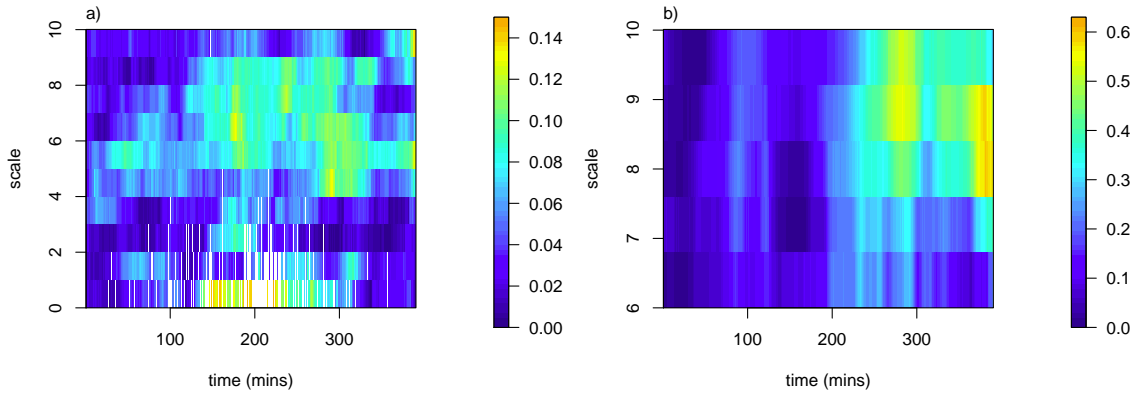

Figure 10: Coherence between Google and Baidu using methods from Section 3.2: a) computed on different irregular sampling grids; b) computed using one minute averages. Scale gets coarser from bottom upwards.

One usual treatment of such irregular data would be to consider it in terms of the one

minute average returns. The estimated coherence using the aggregated data is shown in Figure 10b), where $J^* = 10$ artificial scales and $T^* = 78$ artificial time intervals (each representing a range of 5 minutes) were used. Notice that finer behaviour details are erased, reflecting the coarser sampling rate of the averaged data, and that spurious coherence is unsurprisingly induced by aggregation.

4   Real nonparametric regression using complex lifting

As with the traditional wavelet and lifting transforms, our proposed complex nondecimated lifting transform can be used for nonparametric regression problems, including those with nonequispaced sampling design. In a nutshell, the proposed smoothing procedure can be described as (i) perform the complex lifting transform of the original data, (ii) combine the real and imaginary coefficients into a statistic to undergo thresholding/shrinkage and (iii) take the inverse lifting transform to obtain the estimated unknown signal. A detailed description and estimator properties are provided in Appendix B (supplementary material).

We briefly illustrate the application of this technique to the ethanol data example from Brinkman (1981) that has been analyzed extensively, see for instance Kovac and Silverman (2000) and Cleveland et al. (1992). The data consist of 88 measurements of NOx exhaust emissions from an automobile test engine, together with corresponding engine equivalence ratios, a measure of the richness of the air/ethanol mix (Kovac and Silverman, 2000; Loader, 1999). Because of the nature of the experiment, the observations are not available at equally-spaced design points, and the variability is larger for low equivalence ratios.

We estimate the ratio-dependent (heteroscedastic) variance using a wavelet domain local estimation procedure similar to that of Kovac and Silverman (2000) and Nunes et al. (2006).

Note that our complex adaptive lifting estimate is very similar to the smoothing spline, and both identify changes in slope around 0.7 and 0.9. However, the magnitude and duration of these effects appear to be different between the two estimates. The real-valued adaptive lifting estimate has an overall similar appearance albeit being less smooth and featuring more abrupt changes that are unlikely to be true features of the process. In this example, the true shape of the ethanol curve is of course unknown, however we believe that it is more likely to be smooth. Hence it is pleasing to see that even visually our estimator does a good
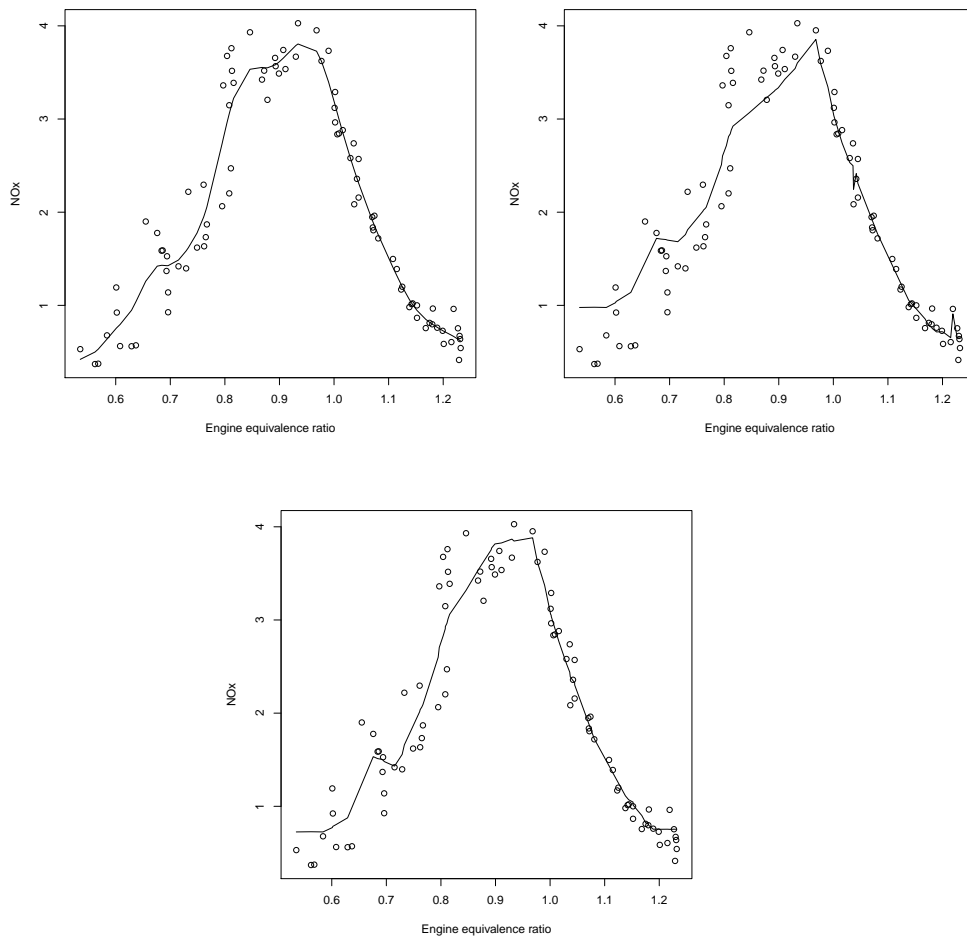
Figure 11: Ethanol data and estimates. Small circles=data; solid line=estimate. Top-left: smoothing spline with cross-validated smoothing parameter; top-right: multiple observation adaptive lifting using $\mathbb{R}$-lift with heteroscedastic variance computation and *EbayesThresh* posterior median thresholding; bottom: $\mathbb{C}$-AP1S with heteroscedastic variance computation and level-dependent soft thresholding.

job in this case.

Supplementary Materials

The supplementary materials contain additional results and comparisons with other methods. The R packages `CNLTreg` and `CNLTtsa` implementing the regression and time series techniques introduced in this article will be released via CRAN in due course.

Acknowledgements

References

Abbas, A. and T. D. Tran (2006). Multiplierless design of biorthogonal dual-tree complex wavelet transform using lifting scheme. In *IEEE International Conference on Image Processing. 2006*, pp. 1605–1608. IEEE.

Abramovich, F., T. Bailey, and T. Sapatinas (2000). Wavelet analysis and its statistical applications. *Journal of the Royal Statistical Society D 49*(1), 1–29.

Allen, J. (1977). Short-term spectral analysis, and modification by discrete fourier transform. *IEEE Transactions on Acoustics Speech and Signal Processing 25*(3), 235–238.

Barber, S. and G. P. Nason (2004). Real nonparametric regression using complex wavelets. *Journal of the Royal Statistical Society B 66*(4), 927–939.

Bos, R., S. de Waele, and P. M. T. Broersen (2002). Autoregressive spectral estimation by application of the Burg algorithm to irregularly sampled data. *IEEE Transactions on Instrumental Measurement 51*(6), 1289–1294.

Brinkman, N. D. (1981). Ethanol fuel-a single-cylinder engine study of efficiency and exhaust emissions. Technical report, SAE Technical Paper.

Broerson, P. M. T. (2008). Time series models for spectral analysis of irregular data far beyond the mean data rate. *Measurement Science and Technology 19*, 1–13.

Cleveland, W., E. Grosse, and W. Shyu (1992). Local regression models. In *Statistical Models in S.* Chambers, J.M. and Hastie, T.J. (eds).

Engle, R. F. (2000). The econometrics of ultra-high-frequency data. *Econometrica 68*(1), 1–22.

Erdogan, E., S. Ma, A. Beygelzimer, and I. Rish (2004). Statistical models for unequally spaced time series. In *Proceedings of the 5th SIAM International Conference on Data Mining*. SIAM.

Fernandes, F. C. A., I. W. Selesnick, R. L. C. van Spaendonck, and C. S. Burrus (2003). Complex wavelet transforms with allpass filters. *Signal Processing 83*(8), 1689–1706.

Foster, G. (1996). Wavelets for period analysis of unevenly sampled time series. *The Astronomical Journal 112*(4), 1709–1729.

Frick, P., A. Grossman, and P. Tchamitchian (1998). Wavelet analysis for signals with gaps. *Journal of Mathematical Physics 39*, 4091–4107.

Gençay, R., M. Dacorogna, U. A. Muller, O. Pictet, and R. Olsen (2001). *An Introduction to High-Frequency Finance*. Academic press.

Hall, P. and P. Patil (1996). On the choice of smoothing parameter, threshold and truncation in nonparametric regression by non-linear wavelet methods. *Journal of the Royal Statistical Society B*, 361–377.

Jacobsen, E. and R. Lyons (2003). The sliding DFT. *IEEE Signal Processing Magazine 20*(2), 74–80.

Jansen, M., G. Nason, and B. Silverman (2001). Scattered data smoothing by empirical bayesian shrinkage of second generation wavelet coefficients. In M. Unser and A. Aldroubi (Eds.), *Wavelet Applications in Signal and Image Processing IX*, Volume 4478, pp. 87–97. SPIE.

Jansen, M., G. P. Nason, and B. W. Silverman (2009). Multiscale methods for data on graphs and irregular multidimensional situations. *Journal Of The Royal Statistical Society Series B 71*(1), 97–125.

Jansen, M. H. and P. J. Oonincx (2005). *Second Generation Wavelets and Applications*. Springer Science & Business Media.

Kingsbury, N. (1999). Image processing with complex wavelets. *Philosophical Transactions of the Royal Society of London A: Mathematical, Physical and Engineering Sciences 357*(1760), 2543–2560.

Kingsbury, N. (2001). Complex wavelets for shift invariant analysis and filtering of signals. *Applied and Computational Harmonic Analysis 10*(3), 234–253.

Knight, M. I. and G. P. Nason (2009). A 'nondecimated' lifting transform. *Statistics and Computing 19*, 1–16.

Knight, M. I. and M. A. Nunes (2012). *nlt: a nondecimated lifting scheme algorithm*. R package version 2.1-3.

Knight, M. I., M. A. Nunes, and G. P. Nason (2012). Spectral estimation for locally stationary time series with missing observations. *Statistics and Computing 22*(4), 877–895.

Kovac, A. and B. W. Silverman (2000). Extending the scope of wavelet regression methods by coefficient-dependent thresholding. *Journal of the American Statistical Association 95*(449), 172–183.

Lina, J.-M. and M. Mayrand (1995). Complex Daubechies wavelets. *Applied and Computational Harmonic Analysis 2*(3), 219–229.

Loader, C. (1999). *Local Regression and Likelihood*. Springer: New York.

Lomb, N. (1976). Least-squares frequency analysis of unequally spaced data. *Astrophysics and Space Science 39*(2), 447–462.

Lütkepohl, H. (2005). *New introduction to multiple time series analysis*. Springer Science & Business Media.

Magarey, J. and N. Kingsbury (1998). Motion estimation using a complex-valued wavelet transform. *IEEE Transactions on Signal Processing 46*(4), 1069–1084.

Nason, G. and B. Silverman (1995). The stationary wavelet transform and some applications. In A. Antoniadis and G. Oppeheim (Eds.), *Wavelets and Statistics*, Volume 103 of *Lecture Notes in Statistics*, pp. 281–300. New York: Springer-Verlag.

Nason, G. P. (2008). *Wavelet Methods in Statistics with R*. Springer.

Nason, G. P., R. von Sachs, and G. Kroisandt (2000). Wavelet processes and adaptive estimation of the evolutionary wavelet spectrum. *Journal of the Royal Statistical Society B 62*(2), 271–292.

Nunes, M. A. and M. I. Knight (2012). *adlift: an adaptive lifting scheme algorithm.*

Nunes, M. A., M. I. Knight, and G. P. Nason (2006). Adaptive lifting for nonparametric regression. *Statistics and Computing 16*(2), 143–159.

Ombao, H., J. Raz, R. von Sachs, and W. Guo (2002). The SLEX model of a non-stationary random process. *Annals of the Institute of Statistical Mathematics 54*(1), 171–200.

Park, T., I. A. Eckley, and H. C. Ombao (2014). Estimating time-evolving partial coherence between signals via multivariate locally stationary wavelet processes. *IEEE Transactions on Signal Processing 62*, 5240–5250.

Percival, D. B. and A. T. Walden (2006). *Wavelet Methods for Time Series Analysis*, Volume 4. Cambridge University Press.

Portilla, J. and E. P. Simoncelli (2000). A parametric texture model based on joint statistics of complex wavelet coefficients. *International Journal of Computer Vision 40*(1), 49–70.

Priestley, M. B. (1983). *Spectral Analysis and Time Series. Volumes I and II in 1 book.* Academic Press.

R Core Team (2013). *R: A Language and Environment for Statistical Computing.* Vienna, Austria: R Foundation for Statistical Computing.

Rehfeld, K., N. Marwan, J. Heitzig, and J. Kurths (2011). Comparison of correlation analysis techniques for irregularly sampled time series. *Nonlinear Processes in Geophysics 18*(3), 389–404.

Reinsel, G. C. (2003). *Elements of multivariate time series analysis*. Springer Science & Business Media.

Sanderson, J. (2010). *Wavelet methods for time series with bivariate observations and irregular sampling grids*. Ph. D. thesis, University of Bristol, UK. `https://www.shef.ac.uk/scharr/sections/heds/staff/hamilton_j`.

Sanderson, J., P. Fryzlewicz, and M. W. Jones (2010). Estimating linear dependence between nonstationary time series using the locally stationary wavelet model. *Biometrika 97*(2), 435–446.

Scargle, J. (1982). Studies in astronomical time series analysis. II- Statistical aspects of spectral analysis of unevenly spaced data. *The Astrophysical Journal 263*, 835–853.

Schröder, P. and W. Sweldens (1996). Building your own wavelets at home. *ACM SIGGRAPH course notes*.

Selesnick, I., R. Baraniuk, and N. Kingsbury (2005). The dual-tree complex wavelet transform. *IEEE Signal Processing Magazine 22*(6), 123–151.

Shui, P.-L., Z. Bao, and Y. Y. Tang (2003). Three-band biorthogonal interpolating complex wavelets with stopband suppression via lifting scheme. *IEEE Transactions on Signal Processing 51*(5), 1293–1305.

Shumway, R. H. and D. S. Stoffer (2013). *Time Series Analysis and its Applications*. Springer Science & Business Media.

Sweldens, W. (1996). The lifting scheme: A custom-design construction of biorthogonal wavelets. *Applied and Computational Harmonic Analysis 3*(2), 186–200.

Vaníček, P. (1971). Further development and properties of the spectral analysis by least-squares. *Astrophysics and Space Science 12*(1), 10–33.

Witt, A. and A. Y. Schumann (2005). Holocene climate variability on millennial scales recorded in greenland ice cores. *Nonlinear Processes in Geophysics 12*(3), 345–352.

Wolff, E. W. (2005). Understanding the past-climate history from Antarctica. *Antarctic Science 17*(04), 487–495.